Porous gravity currents: A survey to determine the joint influence of fluid rheology and variations of medium properties

Accepted in Advances in Water Resources, 30/3/2016

Porous gravity currents: a survey to determine the joint influence of fluid rheology and variations of medium properties

V. Ciriello[a], S. Longo[b], L. Chiapponi[b], V. Di Federico[a]

[a] *Dipartimento di Ingegneria Civile, Chimica, Ambientale e dei Materiali (DICAM), Università di Bologna, Viale Risorgimento, 2, 40136 Bologna, Italy*
[b] *Dipartimento di Ingegneria Civile, Ambiente Territorio e Architettura (DICATeA), Università di Parma, Parco Area delle Scienze, 181/A, 43124 Parma, Italy*

Abstract

We develop a model to grasp the combined effect of rheology and spatial stratifications on two-dimensional non-Newtonian gravity-driven flow in porous media. We consider a power-law constitutive equation for the fluid, and a monomial variation of permeability and porosity along the vertical direction (transverse to the flow) or horizontal direction (parallel to the flow). Under these assumptions, similarity solutions are derived in semi-analytical form for thin gravity currents injected into a two-dimensional porous medium and having constant or time-varying volume. The extent and shape of the porous domain affected by the injection is significantly influenced by the interplay of model parameters. These describe the fluid (flow behaviour index n), the spatial heterogeneity (coefficients $\beta, \gamma, \delta, \omega$ for variations of permeability and porosity in the horizontal or vertical direction), and the type of release (volume exponent α). Theoretical results are validated against two sets of experiments with $\alpha = 1$ (constant inflow) conducted with a stratified porous medium (simulated by superimposing layers of glass beads of different diameter) and a Hele-Shaw analogue for power-law fluid flow, respectively. In the latter case, a recently established Hele-Shaw analogy is extended to the variation of properties parallel to the flow direction. Comparison with experimental results shows that the proposed model is able to capture the propagation of the current front and the current profile.

Keywords: gravity current, porous media, experiment, variable permeability, variable porosity, Hele-Shaw

1. Introduction

Non-Newtonian gravity-driven flow in porous media attracts interest in the context of environmental contamination, as rheological complexity occurs both in environmental contaminants and remediation agents. At the same time, heterogeneity in spatial properties affects the propagation of gravity currents in natural porous media. Gravity currents, generated by the injection of a dense fluid into a light ambient fluid, or vice versa, occur in several natural phenomena and industrial processes [1]. In porous media, the propagation of the current is governed by the interplay between viscous and buoyancy forces, with virtually negligible inertial effects, and it is affected by spatial heterogeneity [2]. Relevant examples include seawater intrusion into coastal aquifers [3], oil recovery [4], penetration of drilling-fluids into surrounding reservoirs [5], and carbon dioxide (CO_2) sequestration in deep subsurface formations [6, 7]. The degree of complexity of models describing porous gravity currents hinges on two main distinctions: first between miscible and immiscible currents, and secondly between confined and unconfined domains. Based on these distinctions, available models to describe the current propagation range from relatively simple analytical schemes, incorporating the sharp-interface approximation and neglecting the motion of the ambient fluid, to full numerical two-phase models incorporating return flows and the effects of diffusion, dispersion, and capillarity. Sharp-interface models are applicable before the transition zone between the two fluids grows too large in case of miscible currents [8], or when the effects of capillarity are negligible for immiscible currents [9]. The motion of the ambient fluid is typically negligible in the unconfined schematization, when the current depth is much less than that of the porous layer; conversely, it becomes important if the thickness of the intruding current is comparable to that of the porous layer [10].

Here we focus on a sharp interface schematization of the gravity current, and consider the case of two fluids whose difference in density generates a gravity-driven flow over a horizontal, rigid and impermeable bed inside a saturated porous domain. Contamination scenarios produced by the spreading of dense nonaqueous phase liquids in groundwater (DNAPL) may fall into this case [11]. From the release source, these substances typically migrate downwards in a shallow phreatic aquifer till the pseudo-impermeable bottom is reached. The conceptualization provided here may describe the subsequent migration of the contaminant.

In several groundwater contamination scenarios, fluids spreading into porous systems exhibit non-Newtonian behavior. Such rheological complexity occurs for: i) the propagation of actual contaminants such as wastewater sludge [12], oil pollutants [13], and waste produced by the resource industries (minerals, coal, and sand-mined oil) [14], and ii) the injection of suspensions employed to enhance the efficiency of in-situ remediation [15, 16, 17]. The relevance of the rheology on gravity currents in porous domains has been already assessed in previous studies. [18, 19] modeled the reference cases of homogeneous infinite domains having plane or axisymmetric geometry, with the intruding fluid described rheologically by the Ostwald-DeWaele power-law formulation. Their model was corroborated by the experiments of [20] in radial geometry. Further modeling advancements were obtained by coupling non-Newtonian rheology with vertical permeability variations in radial geometry [21] and with the effect of channel boundaries [22].

Here we account for the non-Newtonian nature of the intruding fluid and consider at the same time the influence of soil stratification on two-dimensional gravity-driven flow over an horizontal impermeable bottom. An horizontal stratification is modeled with a continuous variation of properties (permeability and porosity) along the vertical direction, in line with the analysis developed by [23] for a Newtonian fluid; the case of two discrete layers was considered by [24]. A vertical stratification, less common but possible in practical applications, is modeled with a continuous variation of permeability and porosity along the horizontal direction [25].

The resulting problem was already analysed in a general frame by Zeldovič & Kompaneec [26] who analyzed the heat equation with heat conductivity and capacity varying as powers of the temperature. A further extensions by Barenblatt [27] treated the self-similar motions of a compressible fluid in a porous medium for plane, cylindrical and spherical geometry. In a subsequent paper, Barenblatt [28] further extended the analysis obtaining limiting self-similar solutions of some special equations, including the classical boundary layer equations. These methods were also earlier employed by [29]. Since these early findings, several papers (e.g., [30, 31, 32] amongst numerous others) used the theory developed by Barenblatt. A detailed exposition of the mathematical theory is contained in the book by Vázquez [33].

The semi-analytical model analyzes the combined influence of rheology and spatial heterogeneity on the propagation of gravity currents in two-dimensional porous domains. Our formulation is aimed at extending previous results describing simplified scenarios with either permeability gradients or

non-Newtonian rheology. A self-similar solution is derived in case of both vertical and horizontal stratifications and for instantaneous or continuous injection. An analysis of the conditions on model parameters required to avoid an unphysical or asymptotically invalid result is presented. A Hele-Shaw analogy is also derived for non-Newtonian power-law flow in two-dimensional porous media for both the configurations analyzed. Model predictions are then assessed against three sets of experiments conducted with two different apparata. A Hele-Shaw cell is used to reproduce simultaneous variations of permeability and porosity along the vertical or horizontal direction. A direct simulation of flow in a stratified packing of glass beads is then conducted to simulate a vertical variation of permeability with constant porosity. In all cases an accurate agreement is obtained between theoretical and experimental results. A set of conclusions closes the paper.

2. Problem formulation

The rheological behavior of a non-Newtonian fluid may be described by several models provided in literature [34]. Among these, the power-law formulation is the simplest one with only two parameters to estimate: the rheological index, n, and the consistency index, $\widetilde{\mu}$. In spite of its simplicity, this model holds in a wide range of shear stress/shear rate values [35]. The Darcy law for a power-law fluid in a porous medium is given by

$$\nabla p - \rho \mathbf{g} = -\frac{1}{\Lambda k^{(n+1)/2}} \left|\mathbf{v}\right|^{n-1} \mathbf{v}. \tag{1}$$

being p the pressure, $\mathbf{g}$ the gravity, $\mathbf{v}$ the Darcy velocity, and k the permeability. In (1) $\Lambda = \Lambda(\phi, \widetilde{\mu}, n) = \frac{8^{(n+1)/2}}{2} \left(\frac{n}{3n+1}\right)^n \frac{\phi^{(n-1)/2}}{\widetilde{\mu}}$, where ϕ denotes the porosity [21].

Consider the power-law fluid spreading as a plane gravity current on a horizontal, rigid and impermeable bed into a saturated porous domain (Figure 1). Motion is driven by the difference in density ($\Delta\rho$) between the lighter fluid, saturating the porous medium, and the heavier intruding fluid. The volume (per unit width) of the intruding fluid is commonly expressed as qt^α, q and α being constants; $\alpha = 0$, and $\alpha = 1$ correspond to constant volume and constant flux injection, respectively.

In a wide range of practical applications it is reasonable to assume: (i) a sharp interface between the two fluids, neglecting mixing, (ii) the intruding current to be thin if compared to its length and to characteristic height h_0

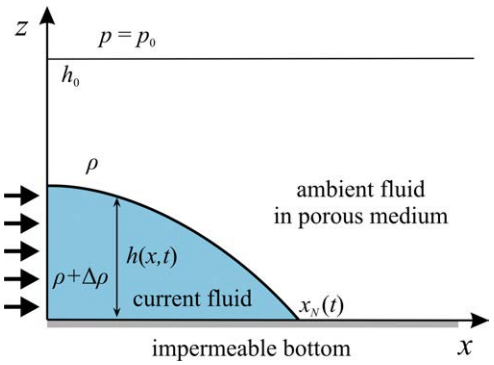

Figure 1: Sketch of a 2-D gravity current intruding into a saturated porous medium.

of the porous medium, and (iii) negligible surface tension effects. When these conditions hold, the current spreading may be simply described by its height $h(x,t)$. The ambient fluid is generally taken to be at rest and vertical velocities in the intruding fluid are neglected. Pressure within the current may be approximated by an hydrostatic distribution, expressed for $z \leq h$ as $p(x,z,t) = p_0 + \Delta\rho\, g(h(x,t) - z) + \rho\, g(h_0 - z)$, where $p_0 = p(z = h_0)$ is a constant. The pressure and the current height are related as $\partial p/\partial x = \Delta\rho\, g(\partial h/\partial x)$.

The local continuity condition, the global mass balance (accounting for the boundary condition in the origin), and the boundary condition at the current front, $x_N(t)$, complete the formulation:

$$\frac{\partial}{\partial x}\left(\int_0^h u\, dz\right) = -\frac{\partial}{\partial t}\left(\int_0^h \phi\, dz\right), \tag{2}$$

$$\int_0^{x_N(t)} \int_0^h \phi\, dz\, dx = q t^{\alpha}, \quad h(x_N(t), t) = 0. \tag{3}$$

Within this framework, it is possible to include deterministic variations in permeability and porosity along the horizontal and vertical direction, in the form of monomial laws reading [36]:

$$\phi(z) = \phi_{0z}(z/x^*)^{\gamma-1}, \quad k(z) = k_{0z}(z/x^*)^{\omega-1}, \tag{4}$$

$$\phi(x) = \phi_{0x}(x/x^*)^{\delta}, \quad k(x) = k_{0x}(x/x^*)^{\beta}, \tag{5}$$

where ϕ_{0x}, ϕ_{0z}, k_{0x}, k_{0z} represent reference values, x^* is a length scale, and γ, ω, δ, and β are real constants. If $\gamma = \omega = 1$ and $\delta = \beta = 0$ the condition of homogeneity is recovered; $\gamma \gtrless 1$ and $\delta \gtrless 0$ entail a porosity increasing/decreasing with (i) vertical distance from the lower impermeable boundary and (ii) horizontal distance from the origin, respectively; $\omega \gtrless 1$ and $\beta \gtrless 0$ entail a similar variation for the permeability. Note that porosity and permeability variations are not independent; in practice, $2 \leq (\omega - 1)/(\gamma - 1) \leq 3$ or $2 \leq \beta/\delta \leq 3$ where $(\omega - 1)/(\gamma - 1) = 2$ and $\beta/\delta = 2$ hold for porous media with tubular fluid paths and $(\omega - 1)/(\gamma - 1) = 3$ or $\beta/\delta = 3$ hold for porous media with intersecting network of cracks or fissures [37, 38]. The actual values of the exponents are subject to other physical limitations as described in the sequel.

Our formulation may be non-dimensionalized by setting $T = t/t^*, X = x/x^*, X_N = x_N/x^*, H = h/x^*, \mathbf{V} = \mathbf{v}/v^*$, where the time, space, and velocity scales t^*, x^*, v^* are collected in Table 1. For $\alpha = 2$, the time scale t^* is no longer valid. This case can be treated defining an additional velocity scale $\tilde{v}^* = (q/\phi_0)^{1/2}$ [39] (where ϕ_0 is a reference porosity), and a new, arbitrary time scale $\tilde{t}^*$; hence, a new spatial length scale $\tilde{x}^* = \tilde{v}^*\tilde{t}^*$ emerges. Dimensionless variables thus become $\tilde{T} = t/\tilde{t}^*$; $\tilde{X} = x/\tilde{x}^*$; $\tilde{X}_N = x_N/\tilde{x}^*$; $\tilde{H} = h/\tilde{x}^*$. In these new dimensionless variables, the problem can be treated following Appendix A in Di Federico et al. [21].

MATH. FORMULATION			Power-law fluid, Graduated medium	Newtonian fluid, Grad. medium, $\gamma=1$ [36]	Power-law fluid, Homogeneous medium [18]
PDE	$\frac{\gamma}{F_1}\frac{v^*}{(x^*)^{F_1-\gamma}}\frac{\partial}{\partial x}\left[h^{F_1}\frac{\partial h}{\partial x}\left\lvert\frac{\partial h}{\partial x}\right\rvert^{1/n-1}\right]=\frac{\partial h^\gamma}{\partial t}$	n	$\in R^+$	1	$\in R^+$
BCs	$h(x_N(t),t)=0;\ \frac{\phi_{0z}}{\gamma(x^*)^{\gamma-1}}\int_0^{x_N(t)}h^\gamma dx=qt^\alpha$	ω	$\in R$	$\in R$	1
ND. PDE	$\frac{\gamma}{F_1}\frac{\partial}{\partial X}\left[H^{F_1}\frac{\partial H}{\partial X}\left\lvert\frac{\partial H}{\partial X}\right\rvert^{1/n-1}\right]=\frac{\partial H^\gamma}{\partial T}$	γ	$\in R^+$	1	1
ND. BCs	$H(X_N(T),T)=0;\ \frac{1}{\gamma}\int_0^{X_N(T)}H^\gamma dX=T^\alpha$	v^*	$\frac{(\Lambda_0\,\Delta\rho\,g)^{1/n}\,k_{0z}^{(n+1)/(2n)}}{\phi_{0z}^{(n+1)/(2n)}}$	$\frac{\Delta\rho\,g k_0}{\phi\mu}$	$\frac{(\Lambda\,\Delta\rho\,g)^{1/n}k_0^{(n+1)/(2n)}}{\phi}$
SIM. VAR.	$\xi=F_1^{F_4}XT^{-F_2}$	t^*	$\left(\frac{q}{\phi_{0z}v^{*2}}\right)^{1/(2-\alpha)}$	$\left(\frac{q}{\phi v^{*2}}\right)^{1/(2-\alpha)}$	$\left(\frac{q}{\phi v^{*2}}\right)^{1/(2-\alpha)}$
SOL.	$H(X,T)=F_1^{F_4/\gamma}\xi_N^{F_5/\gamma}T^{F_3}\Phi(\zeta)$	x^*		v^*t^*	
ODE	$[\Phi^{F_1}\Phi'\,\lvert\Phi'\rvert^{1/n-1}]'+F_2\zeta\Phi^{\gamma-1}\Phi'-F_3\Phi^\gamma=0$	F_1	$\frac{(\omega-\gamma)(n+1)+2\gamma n}{2n}$	ω	1
BCs	$\xi_N=\left(\frac{1}{\gamma}\int_0^1\Phi^\gamma d\zeta\right)^{-1/(F_5+1)},\ \Phi(\zeta=1)=0$	F_2	$\frac{[(\omega-\gamma)(n+1)+2]\alpha+2\gamma n}{(\omega+\gamma)(n+1)+2}$	$\frac{\alpha\omega+1}{\omega+2}$	$\frac{\alpha+n}{2+n}$
add. BC	$\Phi\lvert_{\zeta\to1-\epsilon}=a_0\epsilon^b,\quad \Phi'\lvert_{\zeta\to1-\epsilon}=-a_0b\epsilon^{b-1}$	F_3	$\frac{2[\alpha(n+1)-n]}{(\omega+\gamma)(n+1)+2}$	$\frac{2\alpha-1}{\omega+2}$	$\frac{\alpha(n+1)-n}{2+n}$
		F_4	$\frac{2\gamma n}{(\omega+\gamma)(n+1)+2}$	$\frac{1}{\omega+2}$	$\frac{n}{2+n}$
		F_5	$\frac{2\gamma(n+1)}{(\omega-\gamma)(n+1)+2}$	$\frac{2}{\omega}$	$n+1$

Table 1: Mathematical formulation for a two-dimensional gravity current of power-law fluid intruding a vertically graduated porous medium; expressions for relevant numerical parameters.

Accepted in Advances in Water Resources, 30/3/2016

3. Solution

3.1. Vertical properties variations

If the permeability and porosity variations given by (4) are introduced in (2), the dimensionless governing equation, satisfied by the unknown current profile $H(X,T)$ for $\alpha \neq 2$, is given by

$$\frac{\partial H^\gamma}{\partial T} = \frac{\gamma}{F_1}\frac{\partial}{\partial X}\left(H^{F_1}\frac{\partial H}{\partial X}\left|\frac{\partial H}{\partial X}\right|^{1/n-1}\right), \tag{6}$$

where the expression for the coefficient F_1 (together with the other coefficients introduced in the following) is listed in Table 1.

In non-dimensional form, (3) become, respectively

$$\frac{1}{\gamma}\int_0^{X_N} H^\gamma dX = T^\alpha, \quad H(X_N(T),T) = 0. \tag{7}$$

In order to find similarity solutions, we note that (6)-(7) provide scaling relationships

$$H^{F_1+1/n-\gamma} \sim X^{1/n+1}T^{-1}, \quad H^\gamma X \sim T^\alpha. \tag{8}$$

Eliminating H or X from (8), the scalings for the current length and height result in

$$X \sim T^{F_2}, \quad H \sim T^{F_3}. \tag{9}$$

We therefore introduce the similarity variable and the similarity scaling for the current profile as

$$\xi = F_1^{F_4}T^{-F_2}X, \quad H(X,T) = F_1^{F_4/\gamma}\xi_N^{F_5/\gamma}T^{F_3}\Phi(\zeta), \tag{10}$$

where ξ_N is the unknown value of ξ at the current front, $\Phi(\zeta)$ is the shape function or thickness profile, $\zeta = \xi/\xi_N$ is a rescaled similarity variable. From (10) the extent of the current is given by

$$X_N(T) = \xi_N F_1^{-F_4}T^{F_2}. \tag{11}$$

Substituting (10) in (6)-(7) yields, respectively

$$\left(\Phi^{F_1}\Phi'\left|\Phi'\right|^{1/n-1}\right)' + F_2\zeta\Phi^{\gamma-1}\Phi' - F_3\Phi^\gamma = 0, \tag{12}$$

$$\xi_N = \left(\frac{1}{\gamma} \int_0^1 \Phi^\gamma d\zeta \right)^{-1/(F_5+1)}, \quad \Phi(1) = 0. \tag{13}$$

The analytical model proposed in this section includes, as particular cases, the results derived by (i) Di Federico et al. [18], for a homogeneous medium ($\gamma = \omega = 1$) and any n, (ii) Ciriello et al. [36], for a Newtonian fluid ($n = 1$), $\gamma = 1$ and any ω, (iii) Huppert and Woods [40], for $n = 1, \gamma = 1$ and $\omega = 1$. See Table 1 for details and for the values of the factors F_1 to F_5. The Supplementary Material discusses the conditions on model parameters n, α, ω, and γ, needed for the model to retain its physical significance.

Equation (12) with boundary conditions (13) can be integrated in closed form for the case $\alpha = 0$ (current of constant volume). This allows deriving the following analytical solution:

$$\Phi(\zeta) = \left(\frac{F_{20}^n}{F_5 \gamma^{n-1}} \right)^{F_5/[\gamma(n+1)]} \left(1 - \zeta^{n+1}\right)^{F_5/[\gamma(n+1)]}, \tag{14}$$

$$\xi_N = \left[\frac{1}{\gamma} \left(\frac{F_{20}^n}{F_5 \gamma^{n-1}} \right)^{F_5/(n+1)} \frac{F_5}{(F_5+1)(n+1)} \mathrm{B}\left(\frac{1}{n+1}, \frac{F_5}{n+1} \right) \right]^{-1/(F_5+1)}, \tag{15}$$

where $F_{20} = F_2(\alpha = 0)$ and $\mathrm{B}(\dot{;})$ is the Beta function. For $\omega = \gamma = 1$ and any n, (14) and (15) simplify to equation (23) in Di Federico et al. [18]. For $\gamma = n = 1$ and any $\omega > 0$, (14) and (15) become equations (17)-(18) in Ciriello et al. [36]. For $\omega = \gamma = n = 1$, the result by Huppert and Woods [40] and Pattle [41], $\Phi(\zeta) = (1 - \zeta^2)/6$ and $\xi_N = (9)^{1/3}$, is recovered.

For $\alpha \neq 0$, numerical methods must be employed to solve (12)-(13). A second boundary condition near the front end is introduced to this purpose; in particular, the shape factor is expanded in the Frobenius series for $\zeta \to 1^-$, finding

$$\Phi = a_0(1-\zeta)^b, \quad a_0 = [F_2/(b^{1/n-1}(bF_1+(b-1)/n))]^{bn}, \quad b = 1/(1-n(\gamma-F_1)). \tag{16}$$

Hence,

$$\Phi'(\zeta \to 1) = -a_0 b \epsilon^{b-1}, \tag{17}$$

where $\epsilon = 1 - \zeta$ is a small quantity. The dependence of the shape factor $\Phi(\zeta)$ resulting from numerical integration of (12) with boundary conditions (13)-(17) on model parameters α, n, ω, and γ, and the behaviour of the prefactor $\xi_N(\alpha)$ evaluated by means of (12) are analyzed in the Supplementary Material.

3.2. Horizontal properties variations

In the case of horizontal permeability and porosity variations modeled as (5), the dimensionless governing equation is

$$\frac{\partial H}{\partial T} = \frac{1}{X^{\delta}} \frac{\partial}{\partial X} \left[X^{F_1} H \frac{\partial H}{\partial X} \left| \frac{\partial H}{\partial X} \right|^{1/n-1} \right], \tag{18}$$

where the coefficients are listed in Table 2.

MATH. FORMULATION			Power-law fluid, Graduated medium	Newtonian fluid, Grad. medium [36]	Power-law fluid, Homog. medium, $\delta = 0$ [18]
PDE	$\dfrac{v^*}{(x^*)^{F_1-\delta}}\dfrac{1}{x^\delta}\dfrac{\partial}{\partial x}\left[hx^{F_1}\dfrac{\partial h}{\partial x}\left\lvert\dfrac{\partial h}{\partial x}\right\rvert^{1/n-1}\right]=\dfrac{\partial h}{\partial t}$	n	$\in R^+$	1	$\in R^+$
BCs	$h(x_N(t),t)=0;\quad \dfrac{\phi_{0x}}{(x^*)^\delta}\int_0^{x_N(t)} x^\delta h dx = qt^\alpha$	β	$\in R$	$\in R$	0
ND. PDE	$\dfrac{1}{X^\delta}\dfrac{\partial}{\partial X}\left[HX^{F_1}\dfrac{\partial H}{\partial X}\left\lvert\dfrac{\partial H}{\partial X}\right\rvert^{1/n-1}\right]=\dfrac{\partial H}{\partial T}$	δ	$\in R$	0	0
ND. BCs	$H(X_N(T),T)=0;\quad \int_0^{X_N(T)} X^\delta H dX = T^\alpha$	v^*	$\dfrac{(\Lambda_0\,\Delta\rho\,g)^{1/n}\,k_{0x}^{(n+1)/(2n)}}{\phi_{0x}^{(n+1)/(2n)}}$	$\dfrac{\Delta\rho\,g k_0}{\phi\mu}$	$\dfrac{(\Lambda\,\Delta\rho\,g)^{1/n}k_0^{(n+1)/(2n)}}{\phi}$
SIM. VAR.	$\xi = XT^{-F_2}$	t^*	$\left(\dfrac{q}{\phi_{0x}v^{*2}}\right)^{1/(2-\alpha)}$	$\left(\dfrac{q}{\phi v^{*2}}\right)^{1/(2-\alpha)}$	$\left(\dfrac{q}{\phi v^{*2}}\right)^{1/(2-\alpha)}$
SOL.	$H(X,T)=\xi_N^{F_5}T^{F_3}\Phi(\zeta)$	x^*		v^*t^*	
ODE	$[\zeta^{F_1}\Phi\Phi'\,\lvert\Phi'\rvert^{1/n-1}]'+F_2\zeta^{\delta+1}\Phi'-F_3\zeta^\delta\Phi=0$	F_1	$\dfrac{\delta(n-1)+\beta(n+1)}{2n}$	β	0
BCs	$\xi_N=\left(\int_0^1\zeta^\delta\Phi d\zeta\right)^{-1/(F_5+\delta+1)},\ \Phi(\zeta=1)=0$	F_2	$\dfrac{2(\alpha+n)}{(2-\beta)(n+1)+2+\delta(n+3)}$	$\dfrac{\alpha+1}{3-\beta}$	$\dfrac{\alpha+n}{2+n}$
add. BC	$\Phi\lvert_{\zeta\to1-\epsilon}=F_2^n\epsilon,\quad \Phi'\lvert_{\zeta\to1-\epsilon}=-F_2^n$	F_3	$\dfrac{\alpha(n+1)(2-\beta-\delta)-2n(\delta+1)}{(2-\beta)(n+1)+2+\delta(n+3)}$	$\dfrac{\alpha(2-\beta)-1}{3-\beta}$	$\dfrac{\alpha(n+1)-n}{2+n}$
		F_4	/	/	/
		F_5	$\dfrac{(n+1)(\delta-\beta+2)}{2}$	$2-\beta$	$n+1$

Table 2: Mathematical formulation for a two-dimensional gravity current of power-law fluid intruding a horizontally graduated porous medium; expressions for relevant numerical parameters.

Accepted in Advances in Water Resources, 30/3/2016

In non-dimensional variables, equations (3) become, respectively

$$\int_0^{X_N} X^\delta H dX = T^\alpha, \quad H(X_N(T), T) = 0. \tag{19}$$

Equations (18) and (19) provide the scaling relationships

$$H^{1/n} X^{[(\beta-\delta-2)(n+1)]/(2n)} \sim T^{-1}, \quad H X^{\delta+1} \sim T^\alpha. \tag{20}$$

Eliminating H or X from (20), the scalings for the current length and height are

$$X \sim T^{F_2}, \quad H \sim T^{F_3}. \tag{21}$$

We therefore introduce the similarity variable and the similarity scaling for the current profile as

$$\xi = X T^{-F_2}, \quad H(X, T) = \xi_N^{F_5} T^{F_3} \Phi(\zeta), \tag{22}$$

where ξ_N is the unknown value of ξ at the current front, $\Phi(\zeta)$ is the shape function or thickness profile, $\zeta = \xi/\xi_N$ is a rescaled similarity variable. From (22) the extent of the current is given by

$$X_N(T) = \xi_N T^{F_2}. \tag{23}$$

Substituting (23) in (18) and in (19) yields

$$\left(\zeta^{F_1} \Phi \Phi' \left|\Phi'\right|^{1/n-1}\right)' + F_2 \zeta^{\delta+1} \Phi' - F_3 \zeta^\delta \Phi = 0, \tag{24}$$

$$\xi_N = \left(\int_0^1 \zeta^\delta \Phi d\zeta\right)^{-1/(F_5+\delta+1)}, \quad \Phi(1) = 0. \tag{25}$$

For a homogeneous medium ($\delta = \beta = 0$) and any n, results by Di Federico et al. [18] are recovered (Table 2). For a Newtonian fluid ($n = 1$), $\delta = 0$ and any β, the case studied in Ciriello et al. [36] is found. For $n = 1, \delta = 0$ and $\beta = 0$, the factors further simplify and results by Huppert and Woods [40] are recovered. Table 2 lists a summary of results and the values of the factors F_1 to F_5. The Supplementary Material discusses the conditions on model parameters n, α, β, and δ, needed for the model to retain its physical significance.

The closed-form solution for an instantaneous release of fluid ($\alpha = 0$) is

$$\Phi(\zeta) = \frac{F_{20}^n}{F_5}\left(1 - \zeta^{F_5}\right), \tag{26}$$

$$\xi_N = \left[\frac{F_{20}^n}{(\delta+1)(\delta+F_5+1)}\right]^{-1/(F_5+\delta+1)}, \tag{27}$$

where $F_{20} = F_2(\alpha = 0)$.

For $\beta = \delta = 0$ and any n, (26) and (27) simplify to Eq. (23) in [18]. For $n = 1, \delta = 0$ and any β , (26) and (27) become Equations (33) and (34) in [36]. For $n = 1$ and $\beta = \delta = 0$, results by [41] are again recovered.

As for the vertically varying permeability and porosity case, for values of $\alpha \neq 0$ a second boundary condition near the front end must be employed to numerically solve (24)-(25). This is obtained by expanding the shape factor in Frobenius series for $\zeta \to 1^-$, finding

$$\Phi = a_0(1 - \zeta), \quad a_0 = F_2^n, \tag{28}$$

and hence

$$\Phi'(\zeta \to 1-) = -F_2^n. \tag{29}$$

The dependence of the shape factor $\Phi(\zeta)$ resulting from numerical integration of (24) with boundary conditions (25) and (29) on model parameters α, n, β, and δ, and the behaviour of the prefactor $\xi_N(\alpha)$ evaluated by means of (25) are analyzed in the Supplementary Material.

We note that the case of vertical variations of porosity/permeability can be reduced to the equation analysed by Barenblatt [27]. The case of horizontal variations can be reduced to Barenblatt's equation only for the special value of $\beta = (5n - 3)/(n + 1)$.

4. Hele-Shaw analogy for non-Newtonian porous flow in heterogeneous media

Hele-Shaw flow has been extensively used as an analogue system to model flow in two-dimensional porous media. The original analogy, valid for Newtonian fluids, is based on the similarity between Poiseuille flow between two parallel plates separated by a small gap of aperture b and Darcy flow in a homogeneous medium of permeability k. The analogy was extended to cells with a variable aperture either in the vertical or horizontal direction; these

cells model heterogeneous porous media with spatially variable properties [23, 25]; the striking result is that the aperture variability entails a monomial spatial variation in both permeability and porosity to ensure similarity, with a fixed dependence between the two laws of variation.

The Hele-Shaw approximation was extended to flow of power-law fluids by [18, 42, 43, 44]. Longo et al. [45] developed an extension of the Hele-Shaw analogy for flow of power-law fluids of behaviour index n, so as to reproduce flows in vertically varying porosity and permeability fields described by (4). The analogy was based on the similarity between the flow in the porous medium and the laminar flow between two plates separated by a gap with half-width W varying along the vertical as $W(z) = b_0 z^r$, with b_0 and r being constant parameters. A slightly modified version of this analogy is used in the present work to interpret the experimental results obtained in Hele-Shaw cells with an aperture varying along the vertical direction z; the full version of the analogy is reported in Appendix.

The analogue of flow in a heterogeneous medium with permeability and porosity variations in the horizontal direction x described by (5) requires considering a Hele-Shaw cell with half-aperture varying as as $W(x) = b_0 x^r$. A further extension of the analogy to cover this case is novel to the best of our knowledge and is explored in the Appendix.

5. Experiments

Our theoretical results are validated against multiple sets of experiments. In fact, the two cases of vertical and horizontal variation of the porous medium properties require a different experimental approach. The first can be reproduced directly by superimposing layers of glass beads of different diameter [21], or indirectly by means of a Hele-Shaw cell with varying aperture; both approaches will be used in the sequel. Horizontal variations, on the other hand, are difficult to reproduce directly in the lab by means of an horizontal gradation; hence property variations in the horizontal direction will be reproduced with the analogue model [e.g., 25]. Note that a layered medium with beads of different diameter accurately reproduces variations in permeability but with homogeneous porosity, while a variable aperture Hele-Shaw cell necessarily accounts for both permeability and porosity gradients, as shown in the previous Section. Hence using both approaches explores a wider range of possible combinations of parameters.

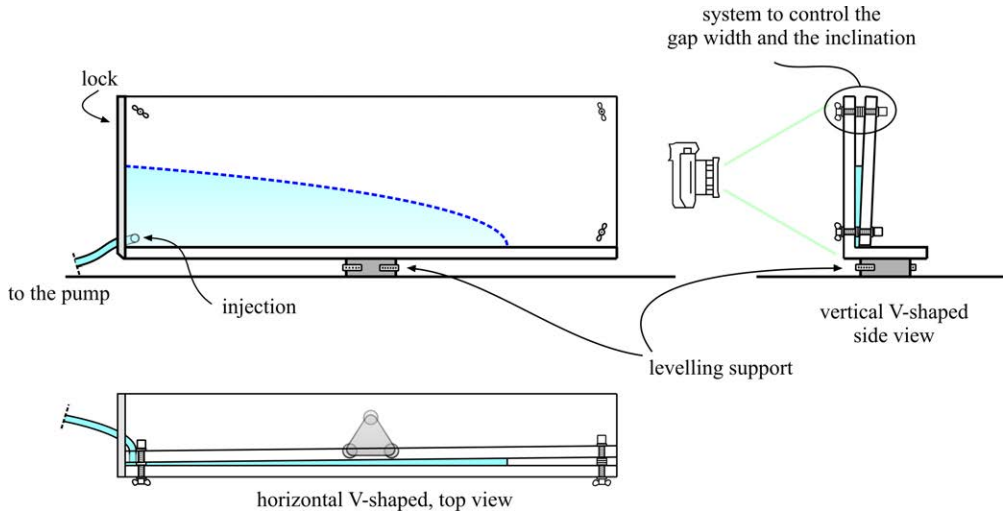

Figure 2: A sketch of the Hele-Shaw cells used for the experiments. The side view refers to the vertically varying gap cell, the top view refers to the horizontally varying gap cell.

5.1. Experimental apparatus and protocol

A schematic of the Hele-Shaw cell is shown in Figure 2. Twelve tests were conducted to verify the theoretical formulation for vertically variable properties. Eight of these used a 75 cm long V-shaped Hele-Shaw cell ($r = 1$) built with two plates of polymethil methacrilate. The distance between the plates could be varied in order to change the coefficient b_0. This setup models a porous medium with $k(z) \propto z^3$ and $\phi(z) \propto z$, mapping with $p = 1$, or $k(z) \propto z^{(4pn+6p-n-3)/(n+1)}$ and $\phi(z) \propto z^{2p-1}$ mapping with $p > 1/2$. The condition $p > 1/2$ is imposed to avoid a reduction of porosity with the distance from the origin, which requires a different analysis. In four additional tests, the plates were set 3 cm apart, obtaining a channel which was filled with glass beads to reproduce directly a porous medium. Four uniform layers of beads, with diameters ranging from 1 to 4 mm and increasing in the vertical direction, were superimposed to reproduce approximately a continuous vertical permeability variation. The thickness of each layer was determined according to the methodology outlined in [21] to obtain the desired values of parameters k_{0z} and ω. This specific setup reproduces a porous medium with a vertical permeability variation ($\omega = 1.63$, corresponding to $k(z) \propto z^{0.63}$) and uniform porosity equal to 0.38.

Six additional tests were conducted to reproduce an horizontal variation of properties, using the same V-shaped tilting the back plate in the horizontal plane. This setup models a porous medium with $k(x) \propto x^3$ and $\phi(x) \propto x$, mapping with $p = 1$, or $k(x) \propto x^{2p+1}$ and $\phi(x) \propto x^{2p-1}$ mapping with $p > 1/2$.

For all tests, a membrane pump with variable frequency was used to deliver a constant flow rate ($\alpha = 1$). The reservoir containing the fluid was placed on an electronic scale (resolution of 0.01 g), and the mass flow delivered was computed as ratio between the weight variation of the reservoir and the duration of the injection. The shear thinning fluids used to conduct the experiments were obtained by mixing water, glycerol and Xantham gum, resulting in two different mixtures with fluid behaviour index $n = 0.43, 0.47$ and consistency index $\widetilde{\mu} = 0.20$, 0.35 $\mathrm{Pa\,s}^n$; the rheological parameters were measured independently with a parallel plate rheometer (Dynamic Shear Rheometer Anton Paar Physica MCR 101). A single experiment was conducted with a Newtonian fluid for calibration purposes. The mass density was measured with a hydrometer (STV3500/23 Salmoiraghi) or by weighing a fixed volume of fluid, with an overall accuracy of 1 %. The profile of the current was detected with photographic techniques [see 20], with an overall accuracy of ± 1.0 mm.

5.2. Experimental results and model interpretation

5.2.1. Vertical variation

Table 3 summarizes the experiments conducted to verify the theoretical formulation for vertically variable properties, and the parameter values for each test. The numerical values taken by the velocity and time scales u^* and t^* are also shown; these vary over more than one order of magnitude. Two videos documenting tests #18 and #20 are available as Supplementary Material.

Figure 3 shows the scaled dimensionless position of the current front as a function of dimensionless time on a double logarithmic scale, with the solid lines indicating the perfect agreement between experiments and theory. Except for early time results, there is a satisfactory collapse of the experimental data onto the theoretical solution in a time range covering three orders of magnitude. Figure 4 and 5 show the comparison between the measured and computed current profile, respectively, for an experiment in a Hele-Shaw cell and in an artificial porous medium. While the early time profile in the cell is still affected by the geometry of the injection (there is a 8 mm plastic pipe

#	ω	γ	b_0	$\widetilde{\mu}$ ($\mathrm{Pa\,s}^n$)	n	ρ ($\mathrm{kg\,m}^{-3}$)	q ($\mathrm{ml\,s}^{-1}$)	u^* ($\mathrm{mm\,s}^{-1}$)	t^* (s)
1	4	2	0.0046875	0.1	1	1230	0.639	6.6	19.8
2	4	2	0.0046875	0.34	0.47	1193	0.296	8.3	10.8
3	4	2	0.0046875	0.34	0.47	1193	0.233	6.7	12.0
13	4	2	0.0046875	0.2	0.45	1100	2.05	47.6	2.1
14	4	2	0.0046875	0.2	0.45	1100	2.28	56.2	1.6
15	4	2	0.0046875	0.2	0.45	1100	0.27	13.9	4.3
19	4	2	0.098	0.34	0.47	1193	0.23	20.0	2.0
20[a]	4	2	0.013473	0.34	0.47	1193	0.28	15.8	1.9
9	1.63	1	-	0.34	0.47	1193	20.46	4.1	4.9
16	1.63	1	-	0.2	0.45	1100	81.33	18.2	1.1
17	1.63	1	-	0.2	0.45	1100	18.6	11.9	0.8
18[a]	1.63	1	-	0.34	0.47	1193	8.65	2.3	4.3

Table 3: Parameter values for the experiments with vertically varying permeability and porosity, conducted in Hele-Shaw cells or vertically graded beads (the last four lines). The symbol a indicates the tests where a video is available as Supplementary Material.

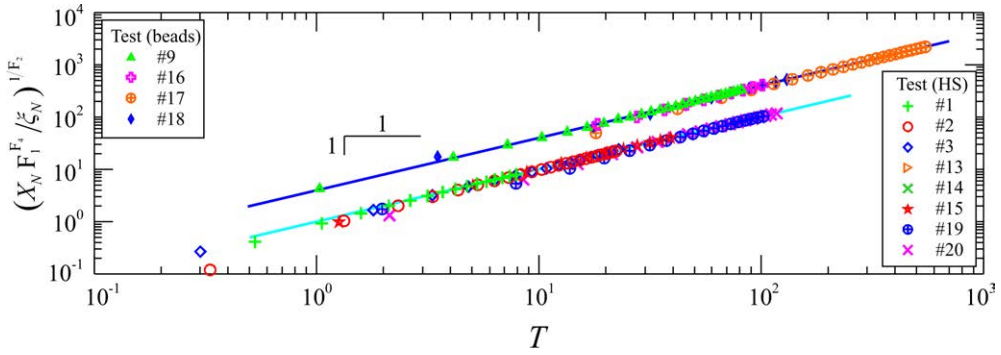

Figure 3: A comparison of theoretical (solid lines) with experimental results (symbols) for vertically varying properties. The dimensionless front position is shown as a function of the dimensionless time for: i) tests in a Hele-Shaw cell (HS) with vertically varying permeability and porosity; ii) tests in a channel filled with vertically graded glass beads (beads) with vertically varying permeability and uniform porosity. For clarity, only one point of every three is plotted. The results for front position in tests with beads have been multiplied by a factor 2, in order that they be separated.

conveying the fluid through a hole in the back wall of the cell, in the left lower corner), with a significant deviation from the theoretical profile, the shape is correctly predicted at intermediate and late times, with minor deviations in the latter case. The experimental profiles for the artificial porous medium show a modest capillary fringe in the upper part of the profile, where the larger beads are located; the capillary fringe near the bottom (where the smallest beads are located) is overcome by the advancing current: the time interval necessary to achieve equilibrium of the capillary fringe for the smallest diameter is much longer than the duration of the test, hence the effects of the fringe are generally modest.

5.2.2. Horizontal variation

Table 4 summarizes the experiments conducted to verify the theoretical formulation for horizontally variable properties, and the parameter values for each test. Again, the numerical values taken by the velocity and time scales u^* and t^* are shown.

Figure 6 shows the scaled dimensionless position of the current front against dimensionless time for this case. Results are similar to Figure 3, showing a good agreement of the experimental data with the theory at in-

#	ω	γ	b_0	$\widetilde{\mu}$ ($\mathrm{Pa\,s}^n$)	n	ρ ($\mathrm{kg\,m}^{-3}$)	q ($\mathrm{ml\,s}^{-1}$)	u^* ($\mathrm{mm\,s}^{-1}$)	t^* (s)
6	3	1	0.002054795	0.34	0.47	1193	0.609	5.2	44.2
7^a	3	1	0.003082192	0.34	0.47	1193	0.6	6.8	25.0
8	3	1	0.003082192	0.34	0.47	1193	0.317	4.6	32.6
10	3	1	0.003082192	0.2	0.45	1100	0.58	13.0	9.2
11	3	1	0.003082192	0.2	0.45	1100	1.59	19.1	8.4
12	3	1	0.003040541	0.2	0.45	1100	1.37	17.6	9.1

Table 4: The input values for the experiments with horizontally varying permeability and porosity in a Hele-Shaw cells. The symbol a indicates the test where video is available as Supplementary Material.

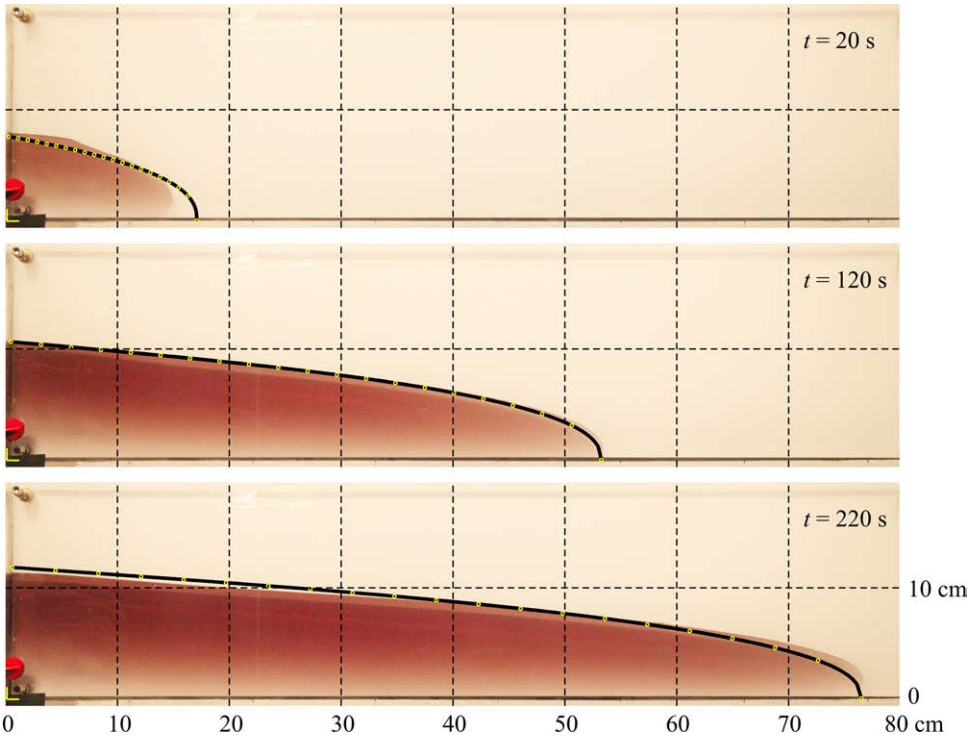

Figure 4: The experimental profile of the current for test #20, with vertically varying permeability and porosity in a V-shaped Hele-Shaw cell. The dashed curve represents the theoretical prediction. Note that the increasing darkness of the current in the vertical is due to the increasing gap of the cell.

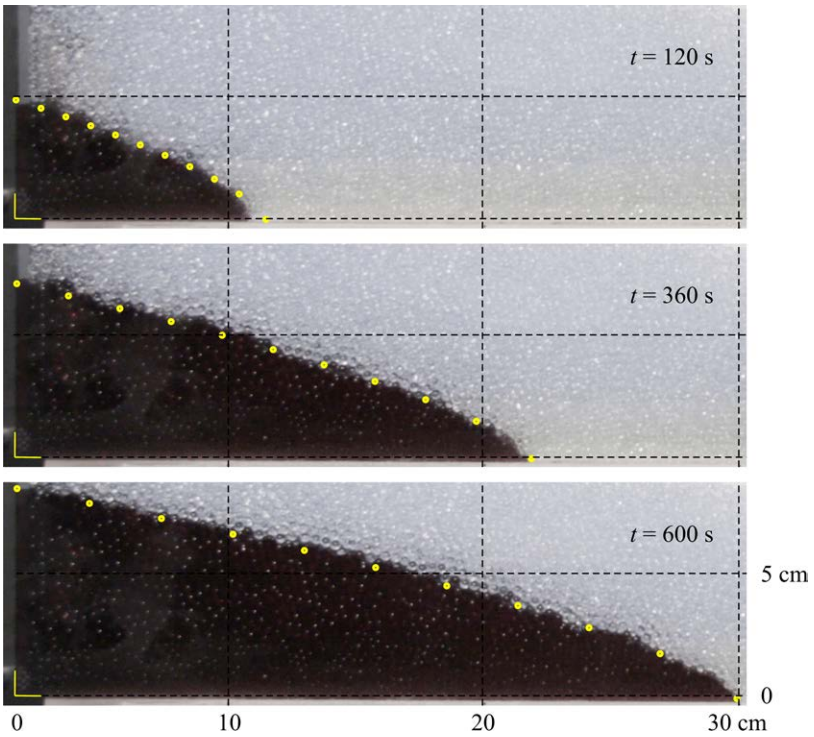

Figure 5: The experimental profile of the current for test #18, with vertically varying permeability and uniform porosity obtained by grading glass beads. The bullets represent the theoretical prediction.

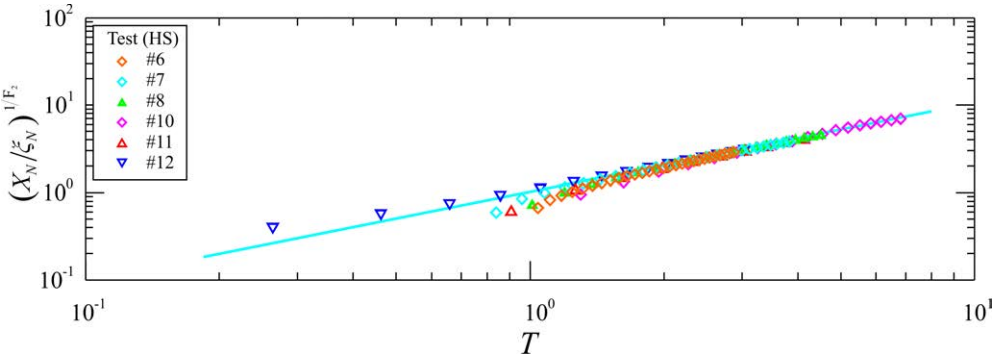

Figure 6: A comparison of theoretical (solid lines) with experimental results (symbols) for horizontally varying properties. The dimensionless front position is shown as a function of the dimensionless time for tests in a Hele-Shaw cell (HS) with horizontally varying permeability and porosity. For clarity, only one point of every three is plotted.

termediate and late times. The tests were performed injecting the fluid in a cross-section of finite gap near the origin of the V-shaped cell, introducing a distortion effect. In comparing experiments and theory, all the data are referred to the virtual origin (where the gap of the cell is zero) and the theoretical profiles require, with respect to the experimental data, a time delay equal to the time required by the current to reach the injection section. However, this correction compensates only partially the distortion effects; hence, a longer time delay is requested and is computed in order to guarantee the best agreement between the theoretical and the experimental profiles, computed via a best fitting procedure. The choice of the injection section represents a compromise between two competing effects, as injecting the fluid near the zero gap origin minimizes the corrections required, but enhances the surface tension effects.

Figure 7 show the comparison between the experimental and the theoretical profile of the current for test #7. The experimental data are influenced by the bottom friction near the front, which becomes dominant if the local thickness of the current is less than the cell width. In this last condition, the model hypotheses are not satisfied since the shear rate in the vertical plane becomes relevant, and a major discrepancy between experiments and theory is expected. The expected disturbing effects of the bottom of the cell reduce the front end speed of the current and locally increase the thickness, respect

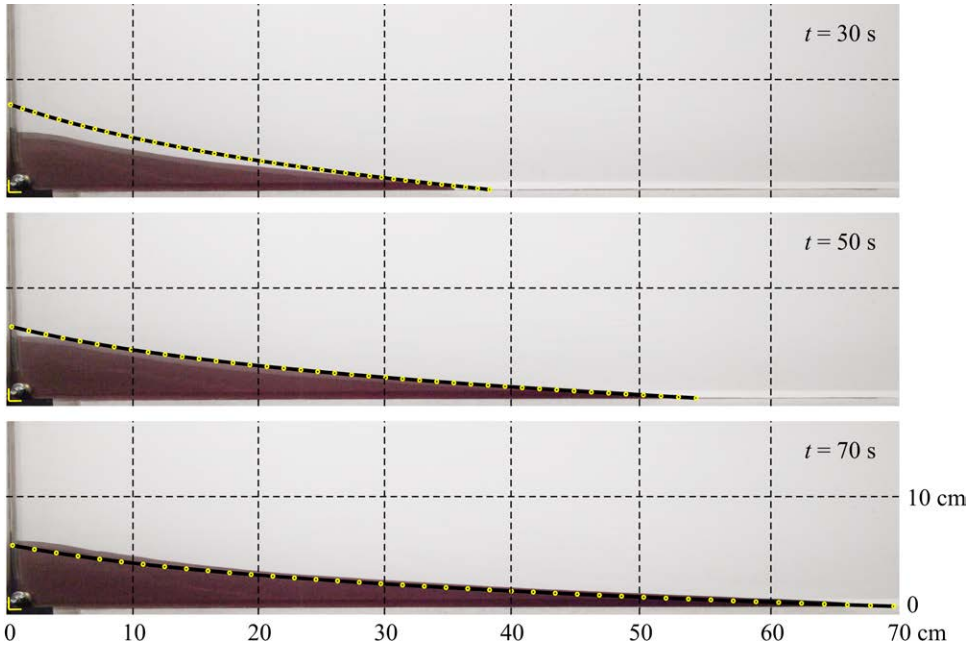

Figure 7: The experimental profile of the current for test #7, with horizontally vaying permeability and porosity. The dashed curve represents the theoretical prediction.

to the undisturbed condition, rendering the analogy invalid at long times.

6. Summary and conclusions

We have developed a sharp-interface model that captures the combined effect of non-Newtonian rheology and spatial variations of permeability and porosity on the evolution of two-dimensional gravity currents spreading into porous media over an horizontal impermeable bottom, due to a time-variable injection. In a simplified framework, the fluid is represented with a power-law rheology, the spatial variations are conceptualized as joint permeability and porosity gradients either perpendicular or parallel to the flow direction, and the volume of the current is taken to vary as a power of time. Scalings are derived for the current front and height as a function of the four model parameters n, describing the fluid rheology, ω and γ (for vertical variations) or β and δ (for horizontal variations) accounting for spatial variability, and α representing the strength of the injection. For certain combinations of

parameters, the solution provided by the model is asymptotically invalid when either the current height increases with time, eventually making the current confined, or the current aspect ratio increases with time, eventually violating the thin current assumption; see the Supplementary Material for a detailed analysis.

We have shown via laboratory-scale experiments that the model is able to reproduce both the extent and the height of the current at intermediate and late times. The experiments were conducted with two different setups: a variable-aperture Hele-Shaw cell, and a glass tank filled with uniform strata of glass beads of different diameter. The first setup was used to reproduce both vertical and horizontal spatial property variations, while the second for vertical permeability variations only. An extension of the Hele-Shaw analogy to power-law fluid flow within porous media with variabile properties was specifically developed.

The propagation rate, thickness and aspect ratio of the current (encapsulated respectively in the factors F_2, F_3, and $F_3 - F_2$) depend on all four model parameters The influence of fluid rheology (consistency and rheological indices) on model results is best discussed in dimensional form, as model scales are themselves function of rheology. The impact of the rheological index n is crucial and can be summarized as follows. For given discharge rate, shear thinning currents propagate always faster than Newtonian or shear thickening currents. The presence of a positive vertical gradient in permeability/porosity reduces this effect: an higher flow behavior index induces a thicker current, which in turn encounters an average reduced flow resistance - the thickness of the current increases less than for a homogeneous porous medium. The opposite is true for the unusual case of a negative vertical gradient of permeability/porosity. In the latter case, shear thinning currents tend to channelize near the bottom, where the average flow resistance is at a minimum. These results were also discussed for a Newtonian fluid current in a two-layered porous media [24]. The horizontal variation of the permeability/porosity is much less important in varying the overall scenario with respect to homogeneous porous media.

Understanding the buoyancy-driven motion of non-Newtonian fluids in porous media provides new insights into environmental contamination issues. In particular, several contaminants infiltrating the subsurface have a complex rheological nature; the same is true for suspensions used as in-situ remediation agents. Our study predicts the time dependence of the volume of subsurface domain invaded by the contaminant or reached by the remedia-

tion agent; the results may be useful for a quick evaluation or benchmarking of numerical models even when the real conditions differ from model assumptions. Future extensions of the model may include the usage of more complex constitutive equation for the fluid, and an improvement in the description of spatial heterogeneity.

7. Acknowledgments

Support from Università di Bologna RFO 2012 and 2013 is gratefully acknowledged. The numerical results used to produce the results of this manuscript are freely available upon request to the corresponding author.

Appendices

A. Hele-Shaw analogy

A.1. Vertical aperture variation

Consider first a cell with half-aperture given by $W(z) = b_0 z^r$, b_0 and r being constants. The spreading in the cell horizontal direction x of a gravity current of a power law fluid is described by

$$\frac{\partial h_{\mathrm{V}}^{r+1}}{\partial t} = \left[\left(\frac{\Delta\rho_{\mathrm{V}}\, g}{\widetilde{\mu}_{\mathrm{V}}} \right)^{1/n_{\mathrm{V}}} \frac{n_{\mathrm{V}}^2 (r+1)}{[r(2n_1+1)+n_{\mathrm{V}}](2n_{\mathrm{V}}+1)} b_0^{(n_{\mathrm{V}}+1)/n_{\mathrm{V}}} \right] \times \frac{\partial}{\partial x} \left[h_{\mathrm{V}}^{1+r(2n_{\mathrm{V}}+1)/n_{\mathrm{V}}} \frac{\partial h_{\mathrm{V}}}{\partial x} \left| \frac{\partial h_{\mathrm{V}}}{\partial x} \right|^{1/n_{\mathrm{V}}-1} \right], \quad \text{(A.1)}$$

where all symbols with subscript $_{\mathrm{V}}$ are the counterparts of those defined for the porous medium. The subscript '$_{\mathrm{V}}$' for the variable H is introduced since a mapping to transform the thickness of the gravity current read in the Hele-Shaw cell into the thickness of the current in the modeled porous medium shall be used. For a Newtonian fluid ($n_{\mathrm{V}} = 1$) and a V-Shaped cell ($r = 1$), (A.1) reduces to Eq. 2.8 in [23]. Eq. (A.1) is solved with the boundary condition at the front end $h_{\mathrm{V}}(x_N(t), t) = 0$ under the constraint of time-variable volume

$$\frac{2b_0}{r+1} \int_0^{x_N(t)} h_{\mathrm{V}}^{r+1} dx = q_{\mathrm{V}} t^{\alpha}. \quad \text{(A.2)}$$

By introducing the velocity and length scales v_{V}^* and x_{V}^* for the cell, given by

$$v_{\mathrm{V}}^* = \left(\frac{r+1}{2b_0\gamma}q_{\mathrm{V}}\right)^{r(n_{\mathrm{V}}+1)/[\alpha r+n_{\mathrm{V}}(2+r-\alpha+\alpha r)]} \times \left[\left(\frac{\Delta\rho_{\mathrm{V}}\, g}{\widetilde{\mu}_{\mathrm{V}}}\right)^{1/n_{\mathrm{V}}} \frac{n_{\mathrm{V}}^2(r+1)b_0^{(n_{\mathrm{V}}+1)/n_{\mathrm{V}}}p^{1/n_{\mathrm{V}}}}{[r(2n_{\mathrm{V}}+1)+n_{\mathrm{V}}](2n_{\mathrm{V}}+1)}\frac{F_1}{\gamma}\right]^{n_{\mathrm{V}}(r+2-\alpha)/[\alpha r+n_{\mathrm{V}}(2+r-\alpha+\alpha r)]} \tag{A.3}$$

$$x_{\mathrm{V}}^* = \left(\frac{r+1}{2b_0\gamma}q_{\mathrm{V}}\right)^{1/(r+2-\alpha)} (v_{\mathrm{V}}^*)^{\alpha/(\alpha-r-2)}, \tag{A.4}$$

eqs. (A.1–A.2) in non dimensional form become

$$\frac{\partial H_{\mathrm{V}}^{r+1}}{\partial T} = \frac{1}{p^{1/n_{\mathrm{V}}}}\frac{\gamma}{F_1}\frac{\partial}{\partial X}\left[H_{\mathrm{V}}^{1+r(2n_{\mathrm{V}}+1)/n_{\mathrm{V}}}\frac{\partial H_{\mathrm{V}}}{\partial X}\left|\frac{\partial H_{\mathrm{V}}}{\partial X}\right|^{1/n_{\mathrm{V}}-1}\right], \tag{A.5}$$

$$\frac{1}{\gamma}\int_0^{X_N(T)} H_{\mathrm{V}}^{r+1}dX = T^{\alpha}. \tag{A.6}$$

Mapping $H_{\mathrm{V}} \to H^p$ yields

$$\frac{\partial H^{p(r+1)}}{\partial T} = \frac{\gamma}{F_1}\frac{\partial}{\partial X}\left[H^{p[1+r(2n_{\mathrm{V}}+1)/n_{\mathrm{V}}]+(p-1)/n_{\mathrm{V}}}\frac{\partial H}{\partial X}\left|\frac{\partial H}{\partial X}\right|^{1/n_{\mathrm{V}}-1}\right], \tag{A.7}$$

$$\frac{1}{\gamma}\int_0^{X_N(T)} H^{p(r+1)}dX = T^{\alpha}. \tag{A.8}$$

The similarity between the flow in the porous medium (hereafter defined the 'prototype') and the flow in the Hele-Shaw cell (hereafter defined the 'model') requires eqs.(6–7) and eqs. (A.7–A.8) to be identical, hence, equating the exponents yields

$$\begin{cases} \gamma = p(r+1) \\ F_1 = p\left(1 + r\dfrac{2n_{\mathrm{V}}+1}{n_{\mathrm{V}}}\right) + \dfrac{p-1}{n_{\mathrm{V}}} \\ n = n_{\mathrm{V}}. \end{cases} \tag{A.9}$$

The system of equations (A.9) admits the solution

$$\begin{cases} \gamma = p(r+1) \\ \omega = \dfrac{3pr(n+1) + p(n+3) - 2}{n+1} \\ n = n_{\mathrm{V}}, \end{cases} \tag{A.10}$$

or

$$\begin{cases} p = \dfrac{(3\gamma - \omega)(n+1) - 2}{2n} \\ r = \dfrac{\omega(n+1) - \gamma(n+3) + 2}{(3\gamma - \omega)(n+1) - 2} \\ n = n_{\mathrm{V}}. \end{cases} \tag{A.11}$$

The analogy requires the two fluids in the prototype and in the model to have the same behaviour index, possibly with different mass density and/or consistency index. For given values of γ and ω, the exponent r and the mapping parameter p can be evaluated.

A.2. Horizontal aperture variation

Modeling the flow in a heterogeneous medium with permeability and porosity variations in the flow direction requires considering a cell with half-aperture varying as $W(x) = b_0 x^r$. Under the same assumptions of the previous subsection, the height of the current satisfies the equation

$$\frac{\partial h}{\partial t} = \left[\left(\frac{\Delta\rho_{\mathrm{H}}\, g}{\widetilde{\mu}_{\mathrm{H}}} \right)^{1/n_{\mathrm{H}}} \frac{n_{\mathrm{H}}}{2n_{\mathrm{H}}+1} b_0^{(n_{\mathrm{H}}+1)/n_{\mathrm{H}}} \right] \times \frac{1}{x_{\mathrm{H}}^r} \frac{\partial}{\partial x_{\mathrm{H}}} \left[x_{\mathrm{H}}^{r(2n_{\mathrm{H}}+1)/n_{\mathrm{H}}} h \frac{\partial h}{\partial x_{\mathrm{H}}} \left| \frac{\partial h}{\partial x_{\mathrm{H}}} \right|^{1/n_{\mathrm{H}}-1} \right], \tag{A.12}$$

which is to be solved with the boundary condition at the front end $h(x_{N\mathrm{H}}(t), t) = 0$ and respecting the integral constraint

$$2b_0 \int_0^{x_{N\mathrm{H}}(t)} x_{\mathrm{H}}^r h\, dx_{\mathrm{H}} = q_{\mathrm{H}} t^{\alpha}. \tag{A.13}$$

As for the vertical aperture Hele-Shaw cell, the subscript H refers the parameters to the Hele-Shaw cell with horizontal aperture. The subscript is also used for the abscissa x since a mapping to transform the abscissa read in the

Hele-Shaw cell into the abscissa for the flow in porous medium shall be used. By introducing the length and velocity scales $v^*_{\rm H}$ and $x^*_{\rm H}$ for the cell, given by

$$v^*_{\rm H} = \left(\frac{q_{\rm H}}{2b_0 p}\right)^{r(n_{\rm H}+1)/[\alpha r + n_{\rm H}(2+r-\alpha+\alpha r)]} \times \left[\left(\frac{\Delta\rho_{\rm H}\, g}{\widetilde{\mu}_{\rm H}}\right)^{1/n_{\rm H}} \frac{n_{\rm H}}{2n_{\rm H}+1} b_0^{(n_{\rm H}+1)/n_{\rm H}} p^{-1/n_{\rm H}-1}\right]^{n_{\rm H}(r+2-\alpha)/[\alpha r + n_{\rm H}(2+r-\alpha+\alpha r)]} \tag{A.14}$$

$$x^*_{\rm H} = \left(\frac{q_{\rm H}}{2b_0 p}\right)^{1/(r+2-\alpha)} (v^*_{\rm H})^{\alpha/(\alpha-r-2)}, \tag{A.15}$$

where the constant $p > 0$ has been introduced for convenience, in non dimensional form eqs. (A.12–A.13) become

$$\frac{\partial H}{\partial T} = \frac{p^{1+1/n_{\rm H}}}{X^r_{\rm H}} \frac{\partial}{\partial X_{\rm H}} \left[X^{r(2n_{\rm H}+1)/n_{\rm H}}_{\rm H} H \frac{\partial H}{\partial X_{\rm H}} \left|\frac{\partial H}{\partial X_{\rm H}}\right|^{1/n_{\rm H}-1}\right], \tag{A.16}$$

$$p \int_0^{X_{N\rm H}(T)} X^r_{\rm H} H dX_{\rm H} = T^\alpha. \tag{A.17}$$

Mapping $X_{\rm H} \to X^p$ yields

$$\frac{\partial H}{\partial T} = \frac{1}{X^{p(r+1)-1}} \frac{\partial}{\partial X} \left[X^{pr(2n_{\rm H}+1)/n_{\rm H}-(p-1)/n_{\rm H}} H \frac{\partial H}{\partial X} \left|\frac{\partial H}{\partial X}\right|^{1/n_{\rm H}-1}\right], \tag{A.18}$$

$$\int_0^{X_N(T)} X^{p(r+1)-1} H dX = T^\alpha. \tag{A.19}$$

The similarity between prototype and model requires identity between eqs. (18–19) in the main paper and the previous equations (A.18–A.19). Equating the exponents yields

$$\begin{cases} \delta = p(r+1) - 1 \\ F_1 = pr\dfrac{2n_{\rm H}+1}{n_{\rm H}} - \dfrac{p-1}{n_{\rm H}} \\ n = n_{\rm H}. \end{cases} \tag{A.20}$$

The system of equations (A.20) admits the solution

$$\begin{cases} \delta = p(r+1) - 1 \\ \beta = p(3r-1) + 1 \\ n = n_{\mathrm{H}}, \end{cases} \tag{A.21}$$

or

$$\begin{cases} p = \dfrac{4 + 3\delta - \beta}{4} \\ r = \dfrac{\delta + \beta}{4 + 3\delta - \beta} \\ n = n_{\mathrm{H}}. \end{cases} \tag{A.22}$$

Notice that the correspondence between the parameters is independent of the fluid behaviour index. For $p = 1$ results $\delta = r$, $\beta = 3\delta = 3r$, and $n = n_{\mathrm{H}}$. In this case, an assigned aperture variation (r) reproduces in similarity only flows in porous media with $\beta/\delta = 3$ and a V-shaped cell ($r = 1$) models only a linear variation of porosity ($\delta = 1$) and a cubic variation of permeability ($\beta = 3$) in the horizontal direction. By mapping with different values of p, a wider choice of parameter combinations is allowed.

References

[1] H. E. Huppert, Gravity currents: a personal perspective, J. Fluid Mech. 554 (2006) 299–322. doi:10.1017/S002211200600930X.

[2] J. Tecklenburg, I. Neuweiler, M. Dentz, J. Carrera, S. Geiger, C. Abramowski, O. Silva, A non-local two-phase flow model for immiscible displacement in highly heterogeneous porous media and its parametrization, Adv. Wat. Res. 62C (2013) 475–487.

[3] A. Werner, M. Bakker, V. Post, A. Vandenbohede, C. Lu, B. Ataie-Ashtiani, C. Simmons, D. Barry, Seawater intrusion processes, investigation and management: Recent advances and future challenges, Adv. Wat. Res. 51 (2013) 3–26.

[4] R. D. Loubens, T. Ramakrishnan, Analysis and computation of gravity-induced migration in porous media, J. Fluid Mech. 675 (2011) 60–86.

[5] L. Li, D. Lockington, M. Parlange, F. Stagnitti, D.-S. Jeng, J. Selker, A. Telyakovskiy, D. Barry, J.-Y. Parlange, Similarity solution of axisymmetric flow in porous media, Adv. Water Resour. 28 (2005) 1076–1082.

[6] M. Dentz, D. Tartakovsky, Abrupt-interface solution for carbon dioxide injection into porous media, Transp. Porous Med. 79 (2009) 15–27.

[7] J. Nordbotten, H. Dahle, Impact of the capillary fringe in vertically integrated models for CO2 storage, Wat. Resour. Res. 47 (2011) W02537.

[8] M. Szulczewski, R. Juanes, The evolution of miscible gravity currents in horizontal porous layers, J. Fluid Mech. 719 (2013) 82–96.

[9] B. Zhao, C. MacMinn, H. E. Huppert, R. Juanes, Capillary pinning and blunting of immiscible gravity currents in porous media, Wat. Resour. Res. 50 (2014) 7067–7081.

[10] H. E. Huppert, J. A. Neufeld, The fluid mechanics of carbon dioxide sequestration, Ann. Rev. Fluid Mech. 46 (2014) 255–272.

[11] D. M. Anderson, R. M. McLaughlin, C. T. Miller, A sharp-interface interpretation of a continuous density model for homogenization of gravity-driven flow in porous media, Physica D 239(19) (2010) 1855–1866.

[12] D. Mohapatra, S. Brar, R. Tyagi, P. Picard, R. Surampalli, Ferro-sonication and partial ozonation pre-treatment and biotransformation of wastewater sludge for degradation of bisphenol a: Rheology studies, Chem. Eng. Sci. 81 (2012) 20–27.

[13] M. Theodoropoulou, V. Karoutsos, C. Tsakiroglou, Investigation of the contamination of fractured formations by non-Newtonian oil pollutants, Environ. Sci. Technol. 2(4) (2001) 321–334.

[14] D. Boger, Rheology and the resource industries, Chem. Eng. Sci. 64(22) (2009) 4525–4536.

[15] J. Silva, M. Liberatore, J. McCray, Characterization of bulk fluid and transport properties for simulating polymer-improved aquifer remediation, J. Environ. Eng.-ASCE 139 (2013) 149–159.

[16] T. Tosco, F. Gastone, R. Sethi, Guar gum solutions for improved delivery of iron particles in porous media (part 2): Iron transport tests and modeling in radial geometry, J. Contam. Hydrol. 166 (2014) 34–51.

[17] N. Kananizadeh, C. Chokejaroenrat, Y. Li, S. Comfort, Modeling improved isco treatment of low permeable zones via viscosity modification: Assessment of system variables, J. Contam. Hydrol. 173 (2015) 25–37.

[18] V. Di Federico, R. Archetti, S. Longo, Similarity solutions for spreading of a two-dimensional non-Newtonian gravity current, J. Non-Newtonian Fluid Mech. 177–178 (2012) 46–53.

[19] V. Di Federico, R. Archetti, S. Longo, Spreading of axisymmetric non-Newtonian power-law gravity currents in porous media, J. Non-Newtonian Fluid Mech. 189–190 (2012) 31–39.

[20] S. Longo, V. Di Federico, L. Chiapponi, R. Archetti, Experimental verification of power-law non-Newtonian axisymmetric porous gravity currents, J. Fluid Mech. 731, R2 (2013) 1–12.

[21] V. Di Federico, S. Longo, L. Chiapponi, R. Archetti, V. Ciriello, Radial gravity currents in vertically graded porous media: Theory and experiments for Newtonian and power-law fluids, Adv. Wat. Res. 70 (2014) 65–76.

[22] S. Longo, V. Ciriello, L. Chiapponi, V. Di Federico, Combined effect of rheology and confining boundaries on spreading of porous gravity currents, Advances in Water Resources 79 (2015) 140–152. doi:10.1016/j.advwatres.2015.02.016.

[23] Z. Zheng, B. Soh, H. E. Huppert, H. A. Stone, Fluid drainage from the edge of a porous reservoir, J. Fluid Mech. 718 (2013) 558–568.

[24] H. E. Huppert, J. A. Neufeld, C. Strandkvist, The competition between gravity and flow focusing in two-layered porous media, J. Fluid Mech. 720 (2013) 5–14.

[25] Z. Zheng, I. C. Christov, H. A. Stone, Influence of heterogeneity on second-kind self-similar solutions for viscous gravity currents, J. Fluid Mech. 747 (2014) 218–246.

[26] Y. B. Zel'dovič, A. S. Kompaneec, On the theory of propagation of heat with the heat conductivity depending upon the temperature, in: Collection in honor of the seventieth birthday of academician A. F. Ioffe, Izdat. Akad. Nauk SSSR, (1950) 61–71.

[27] G. I. Barenblatt, On self-similar motions of compressible fluids in porous media, Prikl. Mat. Mekh. 16 (1952) 679–698, in Russian.

[28] G. I. Barenblatt, On limiting self-similar motions in the theory of unsteady filtration of a gas in a porous medium and the theory of the boundary layer., Prikl. Mat. Mekh. 18 (1954) 409–414, in Russian.

[29] K. P. Staniukovič, On automodel solutions of equations of hydrodynamics possessing central symmetry, C. R. (Doklady) Acad. Sci. URSS (N.S.) 48 (1945) 310–312.

[30] S. Kamin, Similar solutions and the asymptotics of filtration equations, Arch. Ration. Mech. Anal. 60 (1976) 171–183.

[31] S. Kamin, Source-type solutions for equations of nonstationary filtration, J. Math. Anal. Appl. 63 (1978) 263–276.

[32] J. Vázquez, Barenblatt solutions and asymptotic behaviour for a nonlinear fractional heat equation of porous medium types, J. Eur. Math. Soc. 16 (2014) 769–803. doi:10.4171/JEMS/446.

[33] J. Vázquez, The Porous Medium Equation: Mathematical Theory, Oxford Mathematical Monographs, Clarendon Press, 2007.

[34] R. B. Bird, W. E. Stewart, E. N. Lightfoot, Transport phenomena, John Wiley & Sons, 1960.

[35] S. Longo, V. Di Federico, R. Archetti, L. Chiapponi, V. Ciriello, M. Ungarish, On the axisymmetric spreading of non-Newtonian power-law gravity currents of time-dependent volume: An experimental and theoretical investigation focused on the inference of rheological parameters, J. Non-Newtonian Fluid Mech. 201 (2013a) 69–79.

[36] V. Ciriello, V. Di Federico, R. Archetti, S. Longo, Effect of variable permeability on the propagation of thin gravity currents in porous media, Int. J. Non-Linear Mech. 57 (2013) 168–175.

[37] O. M. Phillips, Flow and Reactions in Porous Rocks, Cambridge University Press, 1991.

[38] F. A. Dullien, Porous Media: Fluid Transport and Pore Structure, Academic Press, 1992.

[39] D. Vella, H. E. Huppert, Gravity currents in a porous medium at an inclined plane, J. Fluid Mech. 555 (2006) 353–362.

[40] H. E. Huppert, A. W. Woods, Gravity-driven flows in porous layers, J. Fluid Mech. 292 (1995) 55–69.

[41] R. E. Pattle, Diffusion from an instantaneous point source with a concentration-dependent coefficient, Q. J. Mechanics Appl. Math. 4 (1959) 407–409.

[42] G. Aronsson, U. Janfalk, On Hele-Shaw flow of power-law fluids, Euro. Jnl of Appl. Math. 3 (1992) 343–366.

[43] L. Kondic, P. Palffy-Muhoray, M. J. Shelley, Models of non-Newtonian Hele-Shaw flow, Phys. Rev. E 54(5) (1996) 4536–4539.

[44] S. E. King, Non-Newtonian gravity currents in Hele-Shaw cells, MSc thesis, University of Bristol (2000).

[45] S. Longo, V. Di Federico, L. Chiapponi, A dipole solution for power-law gravity currents in porous formations, J. Fluid Mech. 778 (2015) 534–551. doi:10.1017/jfm.2015.405.